Støpamo, Fredrik G.; Sulaeva, Irina; Budischowsky, David; Rahikainen, Jenni; Marjamaa, Kaisa; Potthast, Antje; Kruus, Kristiina; Eijsink, Vincent G.H.; Várnai, Anikó

Oxidation of cellulose fibers using LPMOs with varying allomorphic substrate preferences, oxidative regioselectivities, and domain structures

Published in:
Carbohydrate Polymers

DOI:
10.1016/j.carbpol.2024.121816

Published: 15/04/2024

Document Version
Publisher's PDF, also known as Version of record

Carbohydrate Polymers 330 (2024) 121816

Contents lists available at ScienceDirect

Carbohydrate Polymers

journal homepage: www.elsevier.com/locate/carbpol

Oxidation of cellulose fibers using LPMOs with varying allomorphic substrate preferences, oxidative regioselectivities, and domain structures

Fredrik G. Støpamo [a], Irina Sulaeva [b], David Budischowsky [b], Jenni Rahikainen [c], Kaisa Marjamaa [c], Antje Potthast [b], Kristiina Kruus [c,d], Vincent G.H. Eijsink [a], Anikó Várnai [a,*]

[a] Norwegian University of Life Sciences (NMBU), Ås, Norway
[b] University of Natural Resources and Life Sciences (BOKU), Vienna, Austria
[c] VTT Technical Research Centre of Finland, Espoo, Finland
[d] Aalto University, Espoo, Finland

ARTICLE INFO

Keywords:
Cellulose
Enzymatic fiber engineering
AA9 LPMOs
Functional variation
Fluorescence

ABSTRACT

Lytic polysaccharide monooxygenases (LPMOs) are excellent candidates for enzymatic functionalization of natural polysaccharides, such as cellulose or chitin, and are gaining relevance in the search for renewable biomaterials. Here, we assessed the cellulose fiber modification potential and catalytic performance of eleven cellulose-active fungal AA9-type LPMOs, including C1-, C4-, and C1/C4-oxidizing LPMOs with and without CBM1 carbohydrate-binding modules, on cellulosic substrates with different degrees of crystallinity and polymer chain arrangement, namely, Cellulose I, Cellulose II, and amorphous cellulose. The potential of LPMOs for cellulose fiber modification varied among the LPMOs and depended primarily on operational stability and substrate binding, and, to some extent, also on regioselectivity and domain structure. While all tested LPMOs were active on natural Cellulose I-type fibers, activity on the Cellulose II allomorph was almost exclusively detected for LPMOs containing a CBM1 and LPMOs with activity on soluble hemicelluloses and cello-oligosaccharides, for example *Nc*AA9C from *Neurospora crassa*. The single-domain variant of *Nc*AA9C oxidized the cellulose fibers to a higher extent than its CBM-containing natural variant and released less soluble products, indicating a more dispersed oxidation pattern without a CBM. Our findings reveal great functional variation among cellulose-active LPMOs, laying the groundwork for further LPMO-based cellulose engineering.

1. Introduction

Development of novel biodegradable materials from renewable resources and upscaling their production processes are prerequisites of establishing a green economy. Cellulose, a β-(1 → 4)-linked polymer of anhydroglucose units and one of the most abundant biopolymers on earth, is a promising resource to produce such materials, with many potential applications, such as biodegradable plastics, filters, and composite materials (Liu, Shi, Cheng, & He, 2016; Sheldon, 2016). Being a structural component in plant cell walls, cellulose harbors a range of beneficial physico-chemical parameters, such as high tensile strength, low toxicity, and biodegradability (Gupta & Shukla, 2020; Henriksson & Berglund, 2007; Wingren, Galbe, & Zacchi, 2003; Yan, Kasal, & Huang, 2016). In addition to dissolution, depolymerization, or modification of cellulose fibers by chemical means, enzymes have been assessed for the generation of cellulose-based biochemicals, polymers, and biomaterials (Marjamaa & Kruus, 2018).

Oxidation is one of the most common reactions to alter cellulose fiber properties (including charge, swelling, and reactivity) or to enable functionalization and subsequent derivatization of fibers. Of the enzymatic processes, oxidation by laccase with (2,2,6,6-tetramethylpiperidin-1-yl)oxy (TEMPO) as mediator will selectively oxidize the C1 aldehyde to carboxyl, and the C6 hydroxyl to carbonyl, and, to some extent, also carboxyl, groups (Moilanen, Kellock, Várnai, Andberg, & Viikari, 2014). Alternatively, lytic polysaccharide monooxygenases (LPMOs) may oxidize the C1 aldehyde to carboxyl or the C4 hydroxyl to a carbonyl group in scissile β-(1 → 4)-linked glycosidic bonds in cellulose or residual hemicelluloses in cellulose fibers (Várnai, Hegnar, Horn,

* Corresponding author.
E-mail addresses: fredrik.gjerstad.stopamo@nmbu.no (F.G. Støpamo), irina.sulaeva@boku.ac.at (I. Sulaeva), david.budischowsky@boku.ac.at (D. Budischowsky), jenni.rahikainen@vtt.fi (J. Rahikainen), kaisa.marjamaa@vtt.fi (K. Marjamaa), antje.potthast@boku.ac.at (A. Potthast), kristiina.kruus@aalto.fi (K. Kruus), vincent.eijsink@nmbu.no (V.G.H. Eijsink), aniko.varnai@nmbu.no (A. Várnai).

https://doi.org/10.1016/j.carbpol.2024.121816
Received 26 October 2023; Received in revised form 9 January 2024; Accepted 10 January 2024
Available online 15 January 2024

Eijsink, & Berrin, 2021). One main difference between the two enzyme systems is the spontaneous cleavage of polysaccharides after oxidation in the case of LPMOs (Beeson, Phillips, Cate, & Marletta, 2012). LPMO action, therefore, will release shorter oxidized (and also some native) oligosaccharides into solution, which are the result of two chain cleavages happening near each other in the same chain or of a single cleavage close to a chain end (Courtade, Forsberg, Heggset, Eijsink, & Aachmann, 2018). Such events lead to a decrease in fiber yield.

Based on their sequences, LPMOs are divided into auxiliary activity (AA) families 9–11 and 13–17 in the CAZy database (Drula et al., 2022). LPMOs in the AA9 and AA10 families are the best studied and include many enzymes that could be used for cellulose fiber oxidation (Koskela et al., 2019; Loureiro et al., 2021; Moreau et al., 2019; Solhi, Li, Li, Heyns, & Brumer, 2022; Villares et al., 2017). LPMOs are copper-containing redox enzymes that require external reductants (such as ascorbic acid, gallic acid, or cysteine) to reduce the copper cofactor and molecular oxygen or hydrogen peroxide as co-substrate (Bissaro et al., 2017; Eijsink et al., 2019; Phillips, Beeson, Cate, & Marletta, 2011; Quinlan et al., 2011; Vaaje-Kolstad et al., 2010). During catalysis, LPMOs oxidize the C1 carbon (C1-oxidation, generating an aldonolactone in equilibrium with the aldonic acid) or the C4 carbon (C4-oxidation, generating a 4-ketoaldose in equilibrium with the 4-hydroxyaldose) at the scissile glycosidic bonds (Eijsink et al., 2019); see Fig. 1A. Fungal cellulose-active AA9s can either perform both C1- and C4-oxidations (C1/C4-oxidation), with varying preference for one or the other, or exclusively catalyze either C1- or C4-oxidation. The large number of AA9 genes in the genomes of many filamentous fungi and the large sequence variation among AA9 LPMOs (Lenfant et al., 2017) suggest variations in substrate specificity. Next to varying oxidative regioselectivities, it is conceivable that AA9s acting on cellulosic fibers target different sites on the fiber.

In addition to variation in the topology of their relatively flat substrate-binding surfaces, the presence of carbohydrate-binding modules (CBMs) may affect the interaction between LPMOs and their substrates. A considerable fraction of AA9 LPMOs contain a family 1 CBM (CBM1) that will promote binding to specific areas of the cellulose fibers (Lenfant et al., 2017). Improved substrate binding mediated by a CBM has been shown to improve LPMO stability under turnover conditions (Courtade et al., 2018), which can be explained by the higher sensitivity of non-substrate-bound LPMOs to auto-oxidative damage (Bissaro et al., 2017). In terms of the potential role of CBMs in fiber modification, Courtade et al. (Courtade et al., 2018) observed that the presence of a CBM2 in a bacterial (AA10) LPMO increased the release of shorter, soluble oxidized oligosaccharides. They postulated that the CBM leads to more localized oxidation of the substrate surface (i.e., around the anchoring point of the CBM), increasing the chance of cutting the same chain twice.

In plant cell walls, the glycan chains of cellulose are organized in microfibrillar structures with clusters of highly ordered cellulose fibrils separated by amorphous regions (Carpita & McCann, 2020). Native cellulose is referred to as Cellulose I (Cel I), in which the cellulose chains adhere to each other in a parallel fashion. In natural cellulose fibers, the Cel I-type crystalline regions are interspersed with less ordered regions, often referred to as amorphous. When processed using e.g. phosphoric acid, cellulose crystals swell and lose their crystalline structure, and the resulting material is (almost) completely amorphous (Wood, 1988). When treated with NaOH at concentrations larger than 15 %, on the other hand, cellulose fibers transform and recrystallize as Cellulose II (Cel II). The resulting Cel II has an antiparallel chain arrangement (Fig. 1B). The differences in the physico-chemical properties (including specific surface area, polymer chain arrangement, and hydrogen bond network) of the various cellulose types suggest that cellulose-active enzymes with large sequence variations, such as cellulases and LPMOs, will differ in their potential for modifying various cellulose fiber types. As an example, a few LPMOs that prefer amorphous cellulose compared to Cel I have been reported (Li et al., 2021; Østby et al., 2023).

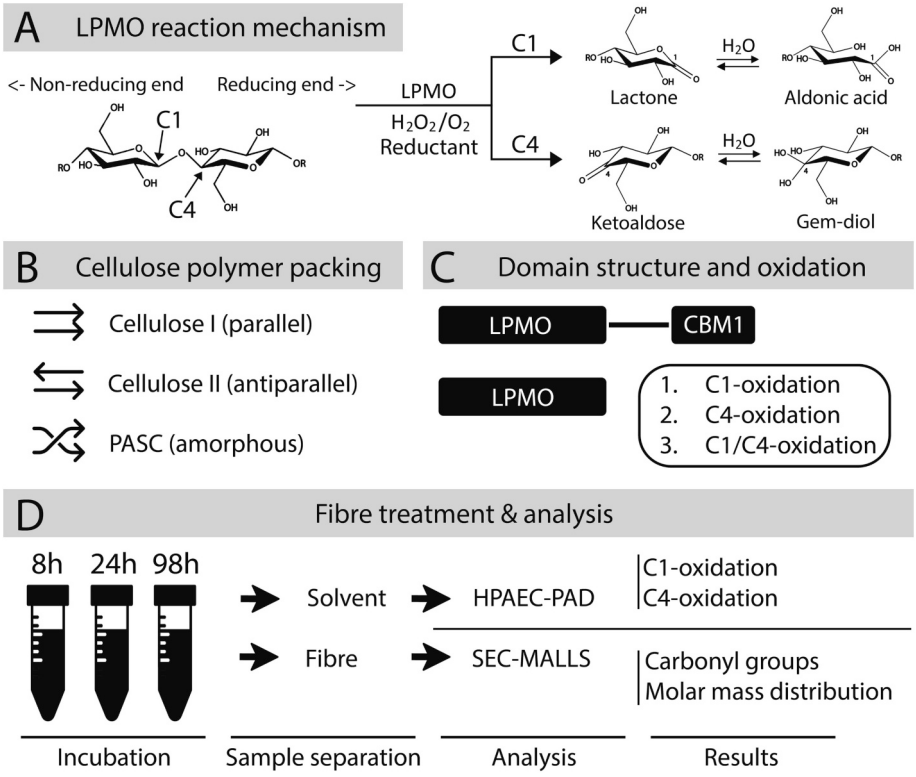

Fig. 1. Experimental scheme. The figure shows the outline of the study, showing (A) possible reaction products, (B) cellulose polymer arrangements in the substrates used, (C) LPMO domain structures and modes of oxidation, and (D) an overview of the various steps in analyzing LPMO functionality. Note that the initial lactone (C1 oxidation) and ketoaldose (C4 oxidation) products are in equilibrium with their hydrated forms, an aldonic acid and a gemdiol, respectively.

Notably, LPMO treatment of native (Cel I)-like cellulose fibers has been shown to aid fiber dissolution for production of regenerated cellulose (Cel II) (Marjamaa et al., 2022), while LPMO-catalyzed oxidation of cellulose after regeneration (Cel II) has not been reported.

To gain insight into functional variation among cellulose-active LPMOs and the impact of the cellulose allomorph on LPMO action, we assessed the potential of eleven cellulose-active fungal LPMOs to oxidize three cellulose types, namely Cel I, Cel II, and amorphous PASC. We evaluated the impact of regioselectivity (i.e., C1-, C4-, and C1/C4-oxidation) and domain structure (with/without CBM) on substrate binding and the extent of fiber modification (Fig. 1C,D). The results reveal large substrate-dependent differences between the tested LPMOs and provide insight into the industrial potential of LPMOs for cellulose modification.

2. Hypotheses

LPMOs are relatively new tools for cellulose fiber engineering. High sequence variation among LPMOs suggests different modes of action, with potential impact on fiber molar mass and oxidation patterns. Here, we assessed if such variation indeed exists, analyzing in detail both LPMO impact on the fiber fraction and soluble products, which is seldom done in the field. Showcasing functional diversity among LPMOs is an important step towards fully exploiting their potential in fiber engineering.

3. Material and methods

3.1. Reagents and substrates

General reagents were purchased from Merck Millipore and Sigma-Aldrich, whereas Bacto Yeast Extract and Bacto Peptone were supplied by BD Biosciences. Three cellulose types were generated as follows. Whatman No. 1 filter papers were purchased from GE Healthcare (production site, China) and used for the generation of Cel I pulp by cold disintegration of the fibers, essentially as described earlier (Rahikainen et al., 2019), followed by washing the pulp to generate the sodium form (Swerin, Odberg, & Lindström, 1990). Cel II was prepared from dis-integrated Whatman No. 1 cellulose (20 g) by excessive swelling in NaOH [18 % (*w/w*), total volume 1.5 L] for 3 h at room temperature. The slurry was thoroughly washed with deionized water until neutral pH. Amorphous cellulose (PASC) was prepared with orthophosphoric acid as previously described (Zhang, Cui, Lynd, & Kuang, 2006). In brief, dis-integrated Whatman No. 1 cellulose (20 g) was dissolved in ice-cold H_3PO_4 [83 % (*w/w*), total volume 500 mL], and the mixture was vigorously stirred for 1 h. PASC was regenerated after dilution of the mixture with deionized water and thoroughly washed until neutral pH.

The pulp suspensions with different cellulose forms were stored in zip lock plastic bags at 4 °C without drying until further use. Dry matter contents of the pulps were determined using a Sartorius MA37 moisture analyzer (Sartorius Stedim Biotech GmbH, Goettingen, Germany).

3.2. Proteins

Purified AA9 LPMOs from *Thermothielavioides* (earlier *Thielavia*) *terrestris* (*Tt*AA9E; UniProt ID, D0VWZ9), *Lentinus similis* (*Ls*AA9A; UniProt ID, A0A0S2GKZ1), *Thermoascus aurantiacus* (*Ta*AA9A; UniProt ID, G3XAP7), and three unnamed organisms (*un*AA9–1, *un*AA9–2, and *un*AA9–3) were kindly provided by Novozymes (Novozymes A/S, Bagsvaerd, Denmark) and used without further treatment. AA9 LPMOs from *Neurospora crassa*, namely *Nc*AA9C (UniProt ID, Q7SHI8), its truncated variant, *Nc*AA9C-N, and *Nc*AA9F (UniProt ID, Q1K4Q1) were produced and purified in-house as described earlier (Borisova et al., 2015; Kittl, Kracher, Burgstaller, Haltrich, & Ludwig, 2012) using a modified purification protocol for the *Nc*AA9C variants as described below. The enzymes were stored in 50 mM Bis-Tris/HCl buffer (pH 6.5) at 4 °C. AA9 LPMOs from *Trichoderma reesei* (teleomorph *Hypocrea jecorina*; *Tr*AA9A; UniProt ID, G0R6T8) and *Podospora anserina* (*Pa*AA9E; UniProt ID, B2ATL7) were produced and purified in-house as described earlier (Kont et al., 2019; Marjamaa et al., 2023) and stored in 25 mM Na-acetate buffer (pH 5.0) at 4 °C. *Trichoderma reesei* (teleomorph *Hypocrea jecorina*) cellobiohydrolase (*Tr*Cel7A; UniProt ID, G0RVK1) was produced and purified as previously described (Ståhlberg et al., 1996).

Full-length *Nc*AA9C was purified as follows. After adjusting the pH to 4.0 with 100 % acetic acid, the filtered and concentrated culture broth was loaded onto 2 × 5-mL HiTrap SP HP columns (GE Healthcare Bio-Sciences AB, Uppsala, Sweden) with 50 mM Na-acetate pH 4.0 as running buffer (A) and 50 mM Na-acetate pH 4.0 containing 1 M NaCl as elution buffer (B) at 1.5 mL/min. The protein was eluted with a linear gradient of 0–70 % B over 150 mL, and the fractions containing *Nc*AA9C (at ca. 40 % B) were pooled. The buffer was exchanged to 50 mM Na-acetate buffer (pH 5.7) using VivaSpin centrifugal tubes (3000 MWCO PES; Sartorius Stedim Biotech). After adding ammonium sulfate to 35 % saturation level, the sample was loaded on 2 × 5-mL HiTrap Phenyl HP columns (GE Healthcare) with 50 mM Na-acetate pH 5.7 containing ammonium sulfate at 35 % saturation level as running buffer (A) and 50 mM Na-acetate pH 5.7 as elution buffer (B). The protein was eluted with a linear gradient of 0–70 % B over 150 mL at 1.5 mL/min, and the fractions containing the pure protein (at around 50 % B) were pooled, then concentrated and dialyzed against 50 mM Bis-Tris/HCl buffer (pH 6.5) using Vivaspin centrifugal tubes (3000 MWCO PES; Sartorius Stedim Biotech).

Truncated *Nc*AA9C (*Nc*AA9C-N), was purified to homogeneity in a single step as follows. Cells were grown in BMGY medium at 29 °C for five days, with supplementation of 12 mL 85 % glycerol per L of culture medium every 24 h. The concentrated and filtered culture broth was loaded onto 3 × 5-mL HiTrap DEAE FF columns (GE Healthcare) with 20 mM Tris/HCl (pH 8.0) as running buffer, at 2 mL/min, and the flow-through, containing *Nc*AA9C-N, was concentrated and dialyzed against 50 mM Bis-Tris/HCl buffer (pH 6.5) using Vivaspin centrifugal tubes (3000 MWCO PES; Sartorius Stedim Biotech).

Purified *Nc*AA9C, *Nc*AA9C-N, and *Nc*AA9F were Cu^{2+}-saturated in 50 mM Bis-Tris/HCl buffer (pH 6.5) by incubation at 4 °C, for 20 min under vertical rotation, with a three-fold molar excess of $CuSO_4$ (Loose et al., 2014), and excess copper was removed by subsequent size exclusion chromatography. This latter step was performed using a HiLoad™ 16/600 Superdex™ 75 PG column (GE Healthcare) with 50 mM Bis-Tris/HCl buffer (pH 6.5) containing 200 mM NaCl as running buffer. Fractions containing pure LPMO were pooled and subjected to buffer exchange to 50 mM Bis-Tris/HCl buffer (pH 6.5) using 3000 MWCO centrifugal filters with a PES membrane. The resulting solutions of pure, copper saturated protein were filter-sterilized using 0.22-μm-pore-size Millex-GV filters (Merck Millipore, Burlington, MA, USA) and stored at 4 °C.

Protein concentrations were measured using Bradford's method (Bio-Rad protein microassay; Bio-Rad Laboratories, Inc.). The presence of endoglucanase background activity in LPMO preparations was assessed by incubating 1 μM of each LPMO overnight with 1 % (*w/v*) Cel I in 50 mM Bis-Tris/HCl buffer, pH 6.5, at 30 °C, in the absence of an electron donor. Products were analyzed by HPAEC-PAD, as described below. These analyses did not reveal any significant glucanase background activities.

3.3. Characterization of celluloses

The morphology of Cel I and Cel II was qualitatively analyzed using optical microscopy (Olympus BX61, Olympus, Tokyo, Japan). The fibers were dyed with Congo Red solution prior to analysis. The surface area of the fibers was measured with a Micromeritics 3Flex Adsorption Analyzer (Micromeritics Instrument Corp., Norcross, GA, USA) following the Brunauer, Emmett and Teller (BET) theory. Samples for this analysis

were dried using a critical point drying method, using BAL-TEC 030 Critical Point Dryer (BAL-TEC AG/Leica Microsystems, Wetzlar, Germany) via solvent exchange from acetone to liquid carbon dioxide (Ketola et al., 2022). The samples were degassed under vacuum at 105 °C for 4 h prior to the measurement. The adsorption isotherm measurement was carried out with nitrogen gas at −196 °C. The adsorption isotherm was measured until $P/P_0 = 0.5$ relative pressure, which is the ratio of the equilibrium pressure to the saturation pressure. The BET surface area was calculated from the adsorption isotherm using relative pressure $P/P_0 = 0.05–0.3$.

The crystallinity index (CrI) for Cel I and Cel II was analyzed using Fourier-transform infrared (FTIR) spectroscopy as reported earlier (Ling et al., 2019; Röder et al., 2006). PASC was analyzed using solid state nuclear magnetic resonance (NMR) on a Bruker Avance III HD 400 spectrometer (Bruker, Germany) according to Jusner et al. (Jusner et al., 2022). The presence of crystalline parts was monitored in the C-4 signal region of the ^{13}C CP/MAS spectra. The molecular weight distribution and carbonyl content of the fibers were analyzed using size exclusion chromatography (SEC) as described further below.

3.4. Analysis of enzyme adsorption to cellulose

Reactions were set up with 1 % (*w/v*) Cel I, Cel II, or PASC substrate and 2 μM LPMO in 50 mM Bis-Tris/HCl buffer (pH 6.5) and incubated at 30 °C under atmospheric conditions and in the absence of a reductant for 5, 15, 45, or 120 min. For each time point, independent reactions were set up in triplicates. The reactions were stopped by filtration using a 96-well filterplate with 0.2 μm PES membrane and a vacuum manifold (Merck Millipore), and the concentration of free protein was measured by recording absorbance at 280 nm using Eppendorf UVettes® and an Eppendorf Biophotometer D30 (Eppendorf AG, Hamburg, Germany). Standard curves were produced for each LPMO individually (0–2 μM).

3.5. LPMO-catalyzed cellulose oxidation

Cellulose types Cel I, Cel II, and PASC were treated with LPMO in 5 mL reactions set up in 50 mL Falcon tubes. Gallic acid aliquots were prepared in 100 mM concentrations containing 7.6 % dimethyl sulfoxide (DMSO) and kept frozen until one-time usage. The reactions contained 1 % (*w/v*) Cel I, Cel II, or PASC, 0.5 μM LPMO, and 1 mM gallic acid in 50 mM Bis-Tris/HCl buffer (pH 6.5). To ensure stable reactions and avoid enzyme inactivation, we used gallic acid instead of ascorbic acid as reductant, as preliminary experiments showed that, with gallic acid only, most LPMOs stayed active during the 98 h incubation, generating up to 800–1000 μM soluble oxidized products. First, the substrate fibers were submerged in the reaction buffer overnight at 4 °C to ensure fiber hydration. Next, the reactions were initiated by adding LPMO and, subsequently, gallic acid to the substrate suspension. Reaction mixtures were incubated at 30 °C with 250 rpm horizontal shaking. Independent reactions were set up for each timepoint (8, 24, and 98 h). The reactions were terminated by incubating at 99 °C for 5 min.

To monitor the formation of soluble oxidized products, 50 μL samples were withdrawn from the 98 h reactions after 4, 8, 16, 24, 32, 45, and 73 h of incubation. Reactions were stopped by incubating at 99 °C for 5 min and filtered through 0.2 μm PES membranes after which the liquid fractions were stored at −20 °C until further analysis. To obtain the supernatant and the fiber fraction at the endpoint, heat-inactivated reaction mixtures were centrifuged at 5000 *g* and 4 °C for 20 min, and the supernatants were removed by pipetting and kept frozen until further analysis. The fiber pellet was mixed with 5 mL 1 % sodium dodecyl sulphate and incubated at 99 °C for 5 min to remove bound proteins. The fiber suspension was centrifuged again at 5000 *g* and 4 °C for 20 min, and the supernatant was removed carefully by pipetting. The fibers were then washed three times with 5 mL 75 % (*w/v*) EtOH and once with 5 mL Milli-Q water, with centrifuging (at 5000 *g* and 4 °C for 20 min) and then removing the supernatant by pipetting after each round. Finally, the fibers were resuspended in 15 mL 75 % (*w/v*) EtOH and were stored at 4 °C before further analyses. Control reactions were prepared by incubating the fibers without LPMO in 50 mM Bis-Tris/HCl buffer, pH 6.5, without reductant or with 1 mM gallic acid as reductant. In addition, reference fibers without enzyme treatment were directly suspended in 75 % (*w/v*) EtOH.

3.6. Analysis of soluble oligosaccharides

Soluble LPMO products were analyzed and quantified by high-performance anion exchange chromatography with pulsed amperometric detection (HPAEC-PAD) using a Dionex ICS-5000 system (Thermo Scientific, Sunnyvale, CA, USA) equipped with a CarboPac PA200 analytical (3 × 250 mm) and guard (3 × 50 mm) column, using a 26 min gradient protocol previously described (Tuveng et al., 2020). Before analysis, the samples were treated with 1 μM *Tr*Cel7A overnight at 37 °C, to simplify the product mixture to a blend of mainly Glc4gemGlc, Glc4gem$(Glc)_2$, GlcGlc1A, $(Glc)_2$Glc1A, and $(Glc)_3$Glc1A. C1-oxidized standards [GlcGlc1A, $(Glc)_2$Glc1A, and $(Glc)_3$Glc1A] were produced by treating cellotetraose, cellotriose, and cellobiose with the cellobiose dehydrogenase *Mt*CDH from *Myriococcum thermophilum* (Zámocký et al., 2008). C4-oxidized standards [Glc4gem$(Glc)_2$ and Glc4gemGlc] were generated by treating cello-1,4-β-D-pentaose (Megazyme International, Ireland) with C4-oxidizing *Nc*AA9C, as previously described (Müller, Várnai, Johansen, Eijsink, & Horn, 2015).

3.7. Analysis of cellulose fibers

In order to get information on carbonyl group content of the fibers (i.e., the reducing-end aldehyde groups and the 4-keto groups generated by C4-oxidation at the non-reducing end), samples (20–25 mg of dry cellulose) were labeled with the fluorescent label carbazole-9-carboxylic acid [2-(2-aminooxyethoxy)ethoxy]amide (CCOA) according to Röhrling et al. (Röhrling et al., 2002). Subsequently, the labeled cellulose samples were washed with deionized water to remove excess CCOA. Next, the solvent was exchanged from water to dimethylacetamide (DMAc) with overnight stirring in DMAc, and finally the samples were dissolved in DMAc/LiCl [9 % (*w/v*)]. The dissolved samples were subjected to size exclusion chromatography (SEC) with four PLgel MIXED-A columns (20 μm particle size; 7.5 × 300 mm; Agilent) coupled in series, and solutes were analyzed using a multiple-angle laser light scattering (MALLS) detector with argon ion laser (λ = 488 nm; Wyatt Dawn DSP; Wyatt Technology, Santa Barbara, USA), a UV detector (Dionex UVD 340; Dionex GmbH, Idstein, Germany), a fluorescence detector with excitation at 290 nm and emission at 340 nm (TSP FL2000; Thermo Fisher Scientific, Waltham, USA), and a refractive index (RI) detector (Shodex RI-71; Showa Denko K.K., Kawasaki, Japan). The system was built up and operated as detailed earlier (Röhrling et al., 2002). DMAc/LiCl [0.9 % (*w/v*)] filtered through a 0.02 μm filter was used as eluent. The data were evaluated using the Chromeleon 7, Astra 6, and Grams software packages. The molecular weight distribution [number-average (M_n), weight-average (M_w), and z-average (M_z) molar masses (Lansing & Kraemer, 1935)] and the associated polymer-relevant parameters (dispersity, Đ; degree of polymerization, DP) were calculated from the MALLS and RI data (Zimm, 1948), based on a refractive index increment of 0.140 mL/g for cellulose in the eluent, i.e. DMAc/LiCl [0.9 % (*w/v*)]. The dispersity Đ is defined as the ratio of M_w to M_n. The degree of polymerization (DP_n) was calculated by dividing M_n by the mass of dehydrated glucose. The content of carbonyl groups (μmol/g fiber) was calculated by dividing the overall amount of fluorescent signal (corresponding to the CCOA-labeled carbonyl groups) by the sample mass.

Regarding the analysis of fiber properties reported in Table 1, average values and their standard deviations were calculated from analyses of six independent samples. These samples were taken from reactions in which fibers were treated as in the enzyme reactions, but without added LPMO. These reactions were run with or without addition

Table 1
Cellulose properties. The table shows the number-average (M_n), weight-average (M_w), and z-average (M_z) molar masses, the amount of carbonyl groups [C=O (μmol/g)], the dispersity index (Đ), and the number-average degree of polymerization (DP_n) for untreated Cellulose I (Cel I), Cellulose II (Cel II) and amorphous cellulose (PASC). Averages and standard deviations were calculated from analyses of six independent samples as described in the Material and methods.

	Cel I	Cel II	PASC
M_n (kDa)	213.9 ± 2.7	164.9 ± 4.7	65.7 ± 1.2
M_w (kDa)	389.3 ± 4.6	290.2 ± 2.8	115.5 ± 2.2
M_z (kDa)	592.1 ± 4.9	448.4 ± 7.5	181.0 ± 5.6
DP_n	1319 ± 17	1016 ± 29	405 ± 7
Đ	1.82 ± 0.04	1.76 ± 0.05	1.76 ± 0.04
C=O (μmol/g)	0.13 ± 0.10	0.06 ± 0.03	6.43 ± 0.52
CrI (%)	55 % (100 % Cel I, 0 % Cel II)	44 % (1 % Cel I, 99 % Cel II)	< 2 %
BET surface area (m^2/g)	13.6	5.3	n.d.

of gallic acid, for 8, 24, or 98 h, yielding six independent samples in total. Low standard deviations in Table 1 show that the fibers were essentially stable in the absence of enzyme.

SEC analyses of PASC samples were challenging due to an additional peak in the high molar mass region in LPMO-treated samples. The peak may be explained by the remaining high molar mass fraction that is preserved after conversion of Cellulose I to PASC, which affects the calculated statistical values and complicates further data processing. These peaks were manually excluded from relevant chromatograms.

4. Results

4.1. Cellulose substrates

The cellulosic substrates, Cel I, Cel II, and amorphous cellulose (PASC), were prepared from Whatman No. 1 filter paper sheets made of cotton linter pulp. The Cel I and Cel II samples both exhibited fiber-like structures (Fig. 2), with Cel I showing a higher fraction of fibrillar elements. The BET surface area value for the Cel II fibers (5.3 m^2/g) was less than half of that for the Cel I fibers (13.6 m^2/g; Table 1). This may be due in part to the lower extent of fibrillation in the Cel II fibers and in part to the absence of the lumen in the regenerated fibers of Cel II.

Regarding cellulose crystallinity, regeneration of cellulose fibers led to a decrease in CrI (44 % for Cel II) as compared with the original cellulose fibers (55 % for Cel I; see Table 1), which is commonly observed after regeneration of cellulose with high CrI (Revol, Dietrich, & Goring, 1987). Furthermore, FTIR confirmed that the crystalline fraction of Cel I occurred solely in the Cel I form, while the crystalline fraction of Cel II was predominantly in the Cel II form (99 %) with the remaining 1 % being in the Cel I form. On the other hand, the CrI of amorphous cellulose (PASC) was <2 %, as confirmed with solid state ^{13}C CP/MAS NMR spectroscopy. The distinct properties of the three cellulose forms make the selected set of substrates suitable for comparing the ability of LPMOs with various regioselectivity, domain structure, and potentially also substrate specificity to modify distinct cellulose types.

4.2. LPMO binding and activity with Cel I, Cel II, and PASC

Substrate binding and catalytic activity were assessed for eleven LPMOs with varying oxidative regioselectivity and domain structure acting on two cellulose allomorphs (Cel I and Cel II) and amorphous cellulose (PASC). All LPMOs bound to and were active on at least one of the cellulose substrates (Figs. 3, 4, 5, & S1). *un*AA9–2, *un*AA9–3, *Tt*AA9E, *Nc*AA9F, and *Pa*AA9E generated C1-oxidized products, *un*AA9–1, *Ls*AA9A, *Nc*AA9C, and *Nc*AA9C-N generated C4-oxidized products, and *Ta*AA9A and *Tr*AA9A generated both C1- and C4-oxidized products, as confirmed with HPAEC-PAD. Importantly, truncation of the CBM1 domain of *Nc*AA9C did not alter the regioselectivity of the AA9 domain, which is consistent with the results of previous studies of AA9 (Borisova et al., 2015; Chalak et al., 2019; Danneels, Tanghe, & Desmet, 2019; Sun et al., 2021) and AA10 (Courtade et al., 2018; Crouch, Labourel, Walton, Davies, & Gilbert, 2016) LPMOs. The observed oxidative regioselectivities are in accordance with published data.

The binding data showed a general trend in that all LPMOs bound to amorphous cellulose (PASC) to the highest and to Cel II to the lowest extent (Fig. 3; see Fig. S1 for the underlying binding curves). The only LPMO seemingly deviating from this trend in Fig. 3 was *Nc*AA9F. The binding time curves for *Nc*AA9F (Fig. S1) showed that, initially, binding of this LPMO adheres to the trend observed for other LPMOs (i.e., binding to PASC > Cel I > Cel II). However, over time, *Nc*AA9F kept disappearing from the solution in the reactions with Cel I and, more so, Cel II. Combined with the minimal activity of *Nc*AA9F on Cel I and Cel II (Fig. 5), this gradual disappearance from solution indicates that the apparent binding reflects unspecific (cellulose-induced) protein aggregation and precipitation.

All studied LPMOs were able to bind to PASC and Cel I, with the

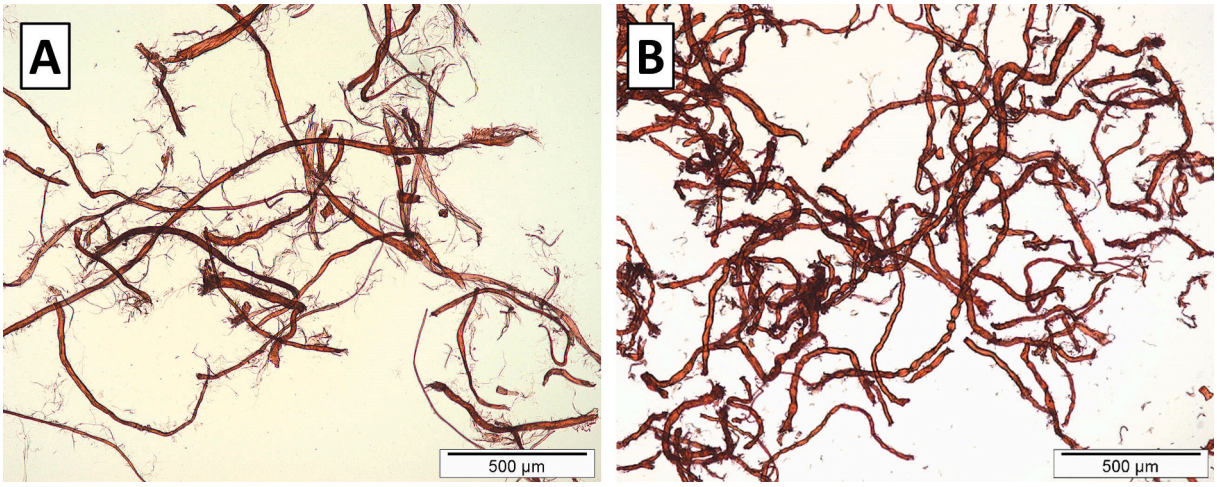

Fig. 2. Light microscopic images of A) Cel I and B) Cel II. Magnification, 40×; scale bars, 500 μm.

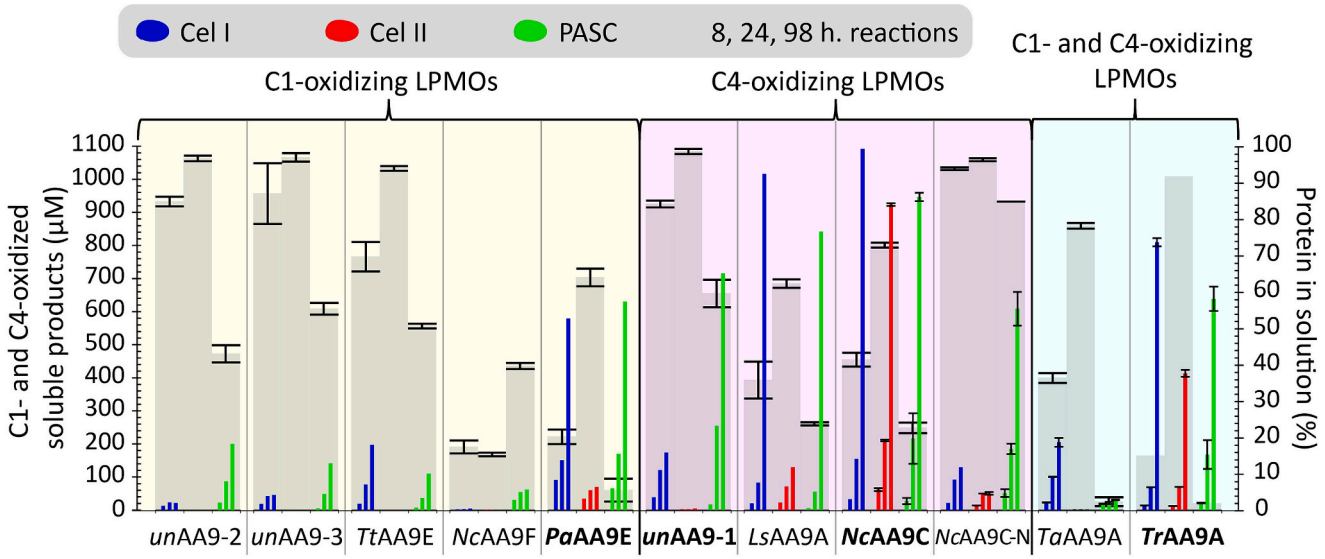

Fig. 3. Generation of soluble products and substrate binding by eleven AA9 LPMOs acting on three cellulose forms. The figure shows the percentage of free protein in solution after incubating 2 µM LPMO with 1 % (*w/v*) substrate at pH 6.5 for 2 h (thick grey bars, right y-axis), and the amount of oxidized soluble products after 8, 24, and 98 h reactions using 1 % (*w/v*) cellulose and 0.5 µM LPMO, supplemented with 1 mM gallic acid (left y-axis) for Cel I (blue bars), Cel II (red bars), and PASC (green bars). Results for C1-, C4-, and C1/C4-oxidizing LPMOs are presented with yellow, pink, and cyan backgrounds, respectively. The names of LPMOs containing a CBM are in bold face. Underlying data appear in Figs. 5 & S1. For reactions that were carried out in duplicate (fiber oxidation) or triplicate (substrate binding) independent reactions, standard deviations are shown with thin black lines. (For interpretation of the references to colour in this figure legend, the reader is referred to the web version of this article.)

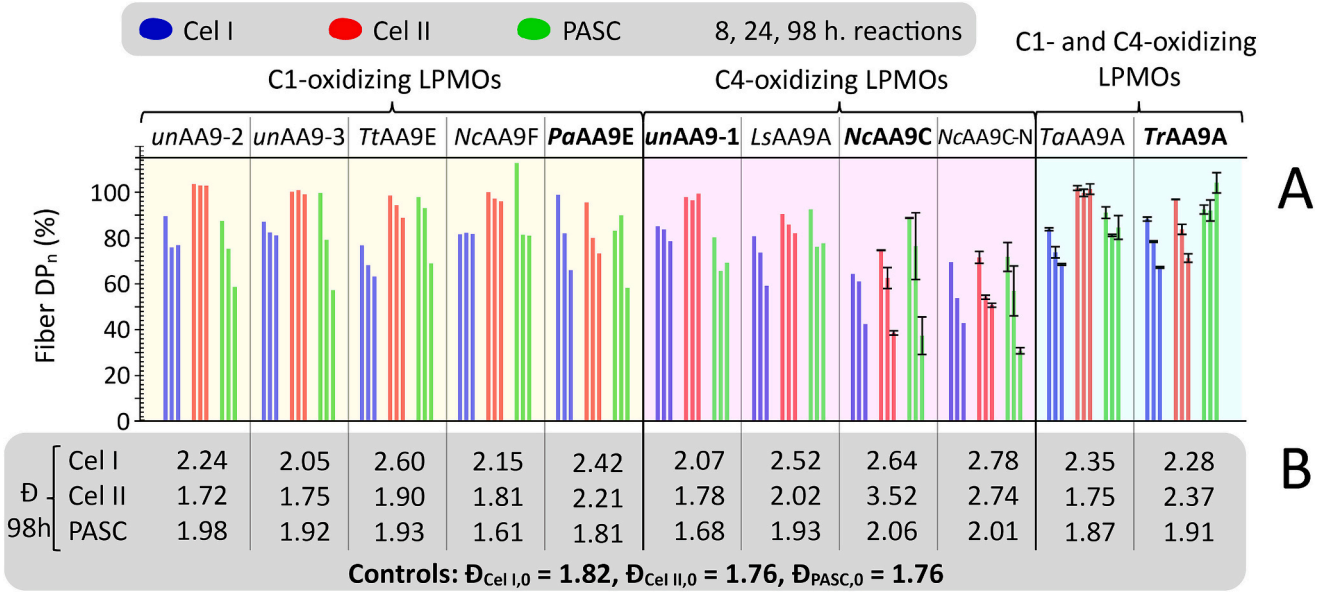

Fig. 4. Impact of eleven AA9 LPMOs on the fiber fraction in reactions with three cellulose forms. Panel A shows the degree of polymerization (DP_n) of the insoluble cellulose fraction after incubating 1 % (*w/v*) Cel I (blue bars), Cel II (red bars), or PASC (green bars) with 0.5 µM LPMO and 1 mM gallic acid for 8, 24, and 98 h reactions. The fiber fractions correspond to the soluble fractions presented in Fig. 3. Results for C1-, C4-, and C1/C4-oxidizing LPMOs are presented with yellow, pink, and cyan backgrounds, respectively. The names of LPMOs containing a CBM are in bold face. DP_n is expressed as % of the (non-changing) DP_n of the material in control reactions, i.e., without LPMO (Table 1). For reactions that were carried out in duplicate (independent reactions), standard deviations are shown with thin black lines. Panel B shows the dispersity (Đ) of the three cellulose types without ("Controls"; at the bottom) and with LPMO treatment after 98 h of incubation. Underlying data appear in Fig. S2. (For interpretation of the references to colour in this figure legend, the reader is referred to the web version of this article.)

exception of the truncated form of *Nc*AA9C (i.e. *Nc*AA9C-N), for which binding to Cel I could not be detected (Figs. 3 & S1). All LPMOs, with the exception of *Nc*AA9F on Cel I, were active on these two substrates, albeit with different efficiencies (Figs. 3 & 4; see below for further discussion). For Cel II, on the other hand, binding was generally lower, and we observed essentially no binding for several LPMOs, which in most cases was accompanied by a lack of activity (Figs. 3 & 5). Of the five studied C1-oxidizing LPMOs, only the one with a CBM (i.e., CBM1), had a clear ability to act on Cel II, showing binding, releasing oxidized products into solution, and decreasing the average fiber length (Figs. 3, 4, & 5; note that the apparent binding of *Nc*AA9F, which is not active on Cel II, likely is an artefact, as discussed above). Our results, however, also show that the presence of a CBM does not guarantee binding to and activity on Cel II. On the one hand, CBM1-containing, C4-oxidizing *Nc*AA9C had the

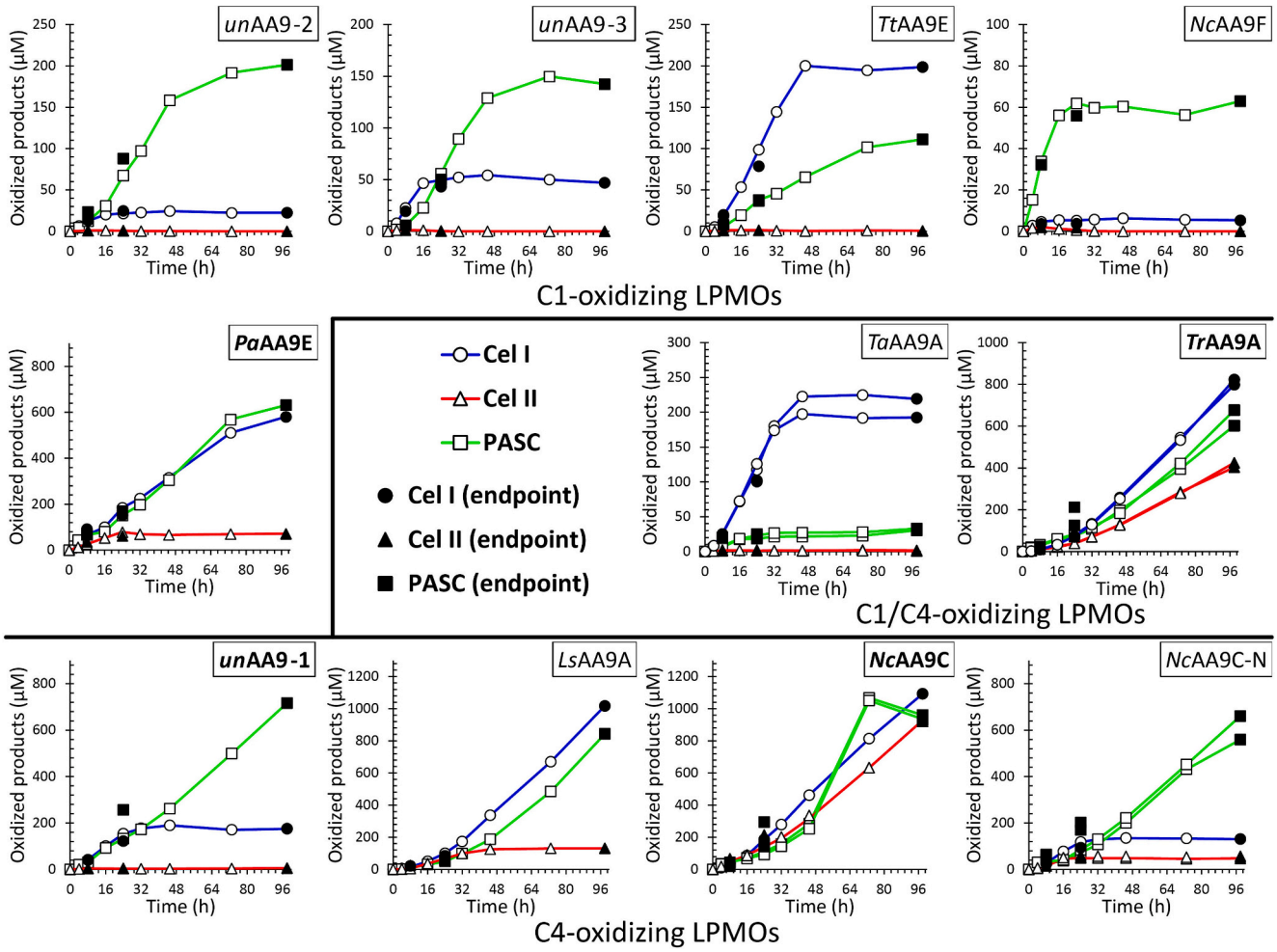

Fig. 5. Formation of soluble oxidized products during LPMO treatment of cellulose fibers. The figure shows the sum of C1- and C4-oxidized soluble products generated upon LPMO treatment of Cel I (circles and blue lines), Cel II (triangles and red lines), and PASC (squares and green lines). The reactions contained 1 % (*w*/*v*) cellulose, 0.5 μM LPMO, and 1 mM gallic acid in 50 mM Bis-Tris/HCl buffer (pH 6.5) and were incubated at 30 °C with shaking at 250 rpm. Filled symbols represent end-point samples of 5 mL reactions incubated for 8 h, 24 h, and 98 h (separate reaction tubes for each time point used to generate Figs. 3 & 4); open symbols represent additional samples taken over time from a 98 h reaction. Duplicate reactions were performed for C1/C4-oxidizing LPMOs with all substrates, and for *Nc*AA9C and *Nc*AA9C-N with Cel II and PASC, and in these cases both datasets are shown. Note the large differences in scaling of the y-axes, which reflect large differences in product levels. LPMOs with CBMs are highlighted in bold, and the regioselectivity (C1, C4, or C1/C4-oxidation) is indicated. (For interpretation of the references to colour in this figure legend, the reader is referred to the web version of this article.)

highest activity on Cel II, whereas CBM1-containing, C4-oxidizing *un*AA9–1 neither showed binding nor activity. This could be taken to suggest variation in the binding properties of the CBM1 modules in these two enzymes. However, importantly, variation in the catalytic domains clearly also plays a role in binding to and activity on Cel II. CBM-truncated *Nc*AA9C (*Nc*AA9C-N) shows reduced binding but still has detectable activity on Cel II. Moreover, single-domain, C4-oxidizing *Ls*AA9A is also active on Cel II.

When comparing all eleven LPMOs acting on all three celluloses, several other trends were observed. Firstly, an apparent higher extent of substrate binding (PASC > Cel I > Cel II; Figs. 3 & S1) corresponded to prolonged activity (i.e., release of oxidized oligosaccharides over a longer period of time; Figs. 4 & 5). This is expected since it is well known that higher affinity for the substrate (or increased substrate concentration) improves LPMO stability under turnover conditions (Courtade et al., 2018). In general, C4-oxidizing AA9s, including *Nc*AA9C and *Ls*AA9A, showed the highest catalytic stability under the studied reaction conditions; these AA9s produced the highest levels of oxidized products and remained active on at least one of the substrates over the 98 h incubation time (Fig. 5). Of all eleven LPMOs, only C4-oxidizing *Nc*AA9C and C1/C4-oxidizing *Tr*AA9A, both with a CBM1, remained active on all three substrates as indicated by a continuous increase in the formation of soluble products throughout the incubation (Fig. 5).

It is noteworthy that the extent of substrate binding did not always correlate with the extent of solubilization of oxidized oligosaccharides. As an example, *Tt*AA9E generated twice as much soluble products from Cel I compared to PASC while this enzyme bound equally well to both substrates. As another example, *Ta*AA9A showed little activity towards PASC despite binding strongly to this substrate. Finally, the data for *Nc*AA9C, the only LPMO that showed strong activity on all three substrates, also revealed discrepancies between the apparent order of binding preferences and the formation of soluble oxidized products (Fig. 3). Such discrepancies between binding and observed activity are not uncommon for characterized LPMOs (Forsberg et al., 2014).

Secondly, the results showed that an increase in the levels of soluble oxidized products over time (Figs. 3 & 5) corresponded with a reduction in the DP_n of the fiber fraction (Figs. 4 & S2). Notably, when soluble product formation halted, no further changes in the DP_n were observed, suggesting that accumulation of soluble products is a good indicator of LPMO activity on the fiber fraction. At the same time, a higher extent of soluble oxidized product formation did not always correspond to a higher reduction in DP_n (Figs. 3 & 4). For example, *Nc*AA9C and its

truncated CBM-free variant, *Nc*AA9C-N, reduced the DP_n of Cel I and Cel II to the same extent, while *Nc*AA9C solubilized higher amounts of oxidized oligosaccharides. Furthermore, *Ls*AA9A, which naturally lacks a CBM, released similar amounts of soluble products from Cel I and PASC as *Nc*AA9C while reducing the DP_n of these substrates to a lesser degree than *Nc*AA9C. Such discrepancies likely relate to different attack patterns on the fibers, since these patterns will determine which fraction of the oxidized products become soluble. All in all, the results shown in Figs. 3, 4, & 5 reveal considerable functional differences between the various LPMOs.

Looking at Cel I and Cel II, the enzymes with the highest impact on fiber DP_n include CBM-containing, C1-oxidizing *Pa*AA9E and CBM-containing C4-oxidizing *Nc*AA9C. The most efficient enzyme, *Nc*AA9C decreased the average DP_n to approximately 40 % of the original value for both cellulose types (Fig. 4). *Ls*AA9A, which is one of the better studied LPMOs (Simmons et al., 2017), was less effective in reducing the DP_n, but nevertheless provides an alternative tool to reduce the DP_n of Cel I and Cel II, while introducing ketones at the C4 position. Regarding C1-oxidation, which leads to incorporation of carboxylic groups on the fiber surface, *Tt*AA9E and *Pa*AA9E showed the highest potential on Cel I (decreasing the DP_n to about 60–70 % of the original value), whereas *Pa*AA9E also seemed efficient on Cel II (decreasing the DP_n to about 70 % of the original value). It is noteworthy that for some of the LPMO-treated PASC samples, the results of SEC-MALLS analysis were disturbed by the presence of an additional peak in the high molar mass area (for an example, see Fig. S3). This peak, which appeared only in a handful of samples (intriguingly, at some of the time points only and not in both duplicates), may be related to leftover protein impurities or potentially explained by the remaining high molar mass fraction of cellulose preserved after Cel I conversion to PASC. Such a high molar mass fraction would lead to higher calculated statistical moments for some samples; *Ls*AA9A-, *Ta*AA9A-, and *Tr*AA9A-treated PASC samples being affected the most.

4.3. *Quantification of fiber oxidation by C4-oxidizing LPMOs*

To further assess the potential of LPMOs in fiber modification, beyond a reduction in the DP_n, we analyzed the extent of fiber oxidation

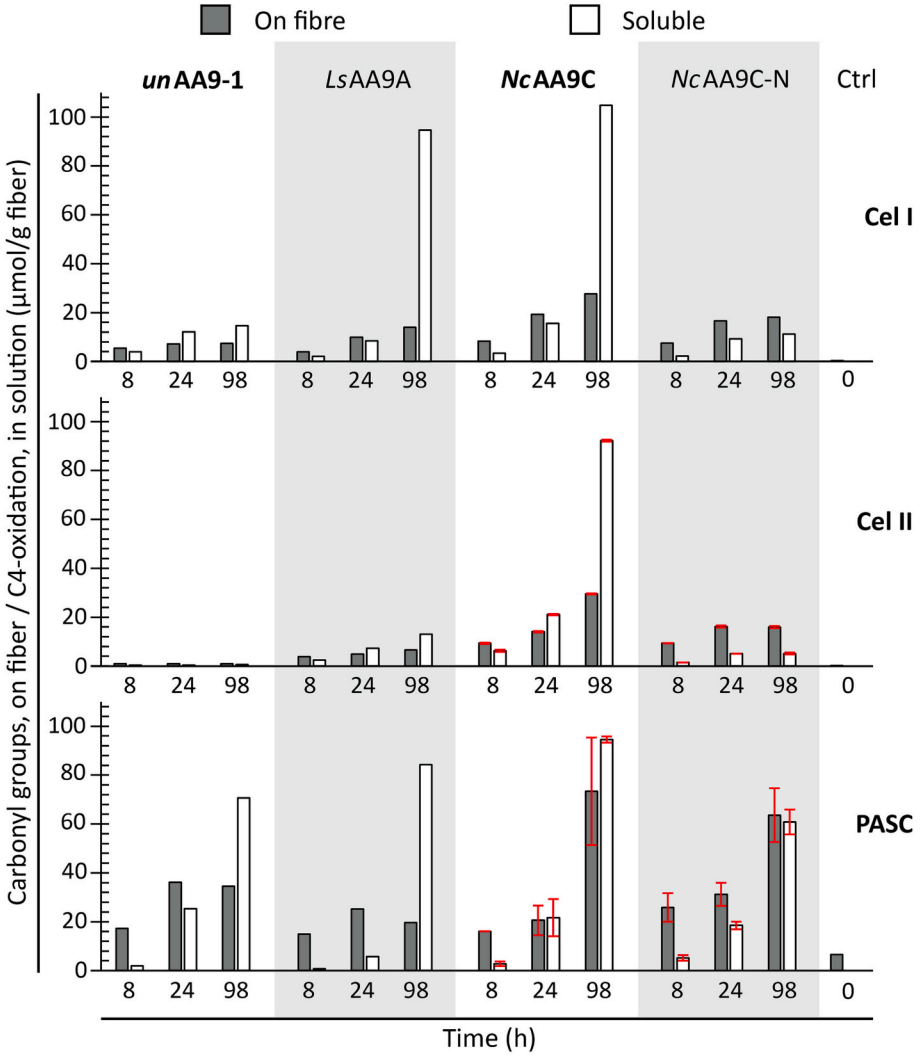

Fig. 6. Formation of carbonyls in the fiber fraction and soluble C4-oxidized products in the reaction supernatant during LPMO treatment of different cellulose types. The fiber (grey bars) and supernatant (white bars) fractions of reactions with C4-oxidizing LPMOs are compared for Cel I (top), Cel II (middle), and amorphous cellulose (PASC, bottom). The carbonyl content in the fiber fraction (grey bars) includes C4 ketones from fiber oxidation by the LPMO and reducing-end aldehydes, whereas C4 oxidation in the supernatant (white bars) includes the amount of C4 ketones generated by LPMO action. The grey background indicates that the LPMO (i.e., *Ls*AA9A and *Nc*AA9C-N) lacks a CBM. The names of LPMOs containing a CBM1 are printed in bold face. Each time point represents an independent reaction. For the time points where two independent reactions were carried out; error bars representing standard deviations are shown in red. (For interpretation of the references to colour in this figure legend, the reader is referred to the web version of this article.)

with a recently developed method that is based on complete dissolution of cellulose fibers and subsequent selective detection of carbonyl groups (C4-oxidation and reducing-end aldehydes) but not carboxyl groups (C1-oxidation) (Röhrling et al., 2002; Sulaeva et al., 2023). Thus, we zoomed in on the action of C4-oxidizing LPMOs. The results (Fig. 6) again show considerable differences between the LPMOs. For example, for some LPMOs, fiber cleavage started slowing down early on in the reaction, while shorter oxidized products continued to be released into solution. This effect is visible for several LPMOs acting on several substrates and indicates that there is a limit to the number of cleavage sites in the fibers. Regions once attacked by the LPMO will be re-attacked, leading to the release of soluble products. Reactions with *un*AA9–1 or *Nc*AA9C-N indicated catalytic inactivation in reactions with Cel I and Cel II as accumulation of oxidized products stagnated after 8 h (for *un*AA9–1) or 24 h (*Nc*AA9C-N) in both the supernatant and fiber fractions (Fig. 6). Importantly, the accumulation of carbonyl groups in the fiber and solubilized fractions and the halt thereof corresponded with a decrease and the stagnation of such decrease in the DP_n (Figs. 4 & 6), respectively, confirming that oxidative cleavage of cellulose led to the observed decrease in DP_n.

Overall, PASC fibers were oxidized to the highest extent, showing 19–73 μmol carbonyl groups/g fiber at the end of the 98 h incubation, followed by Cel I (7–28 μmol/g) and Cel II (1–29 μmol/g). The fact that PASC was oxidized to a higher extent than Cel I and Cel II may be related to its higher specific surface area as well as the fact that all four C4-oxidizing enzymes remained active on PASC throughout the 98 h reaction time (as indicated by the continuous accumulation of soluble products; Fig. 5).

It is worth noting the difference between the most effective of all tested LPMOs, *Nc*AA9C, and its truncated, CBM-free variant, *Nc*AA9C-N. In terms of oxidation of Cel I and Cel II, the two enzyme variants were similarly effective up to 24 h, while the truncated variant released substantially less oxidized products into solution. After 24 h, product formation by the truncated enzyme levelled off, indicative of enzyme inactivation. On PASC, on the other hand, *Nc*AA9C-N remained active over the 98 h incubation period. In the reactions with PASC, *Nc*AA9C-N generated product levels similar to those generated by *Nc*AA9C, and product levels increased considerably between 24 h and 98 h for both enzymes, although the truncated enzyme did show lower product levels after 98 h. Notably, the truncated enzyme seemed slightly more efficient early on in the reaction, especially regarding oxidation of the fiber fraction (Fig. 6). These observations provide interesting insight into the role of the CBM, as discussed below.

4.4. Impact of the cellulose type on the ratio of C1- and C4-oxidized products generated by LPMOs with mixed C1/C4-oxidizing regioselectivity

Next, we assessed if the cellulose type had an impact on the ratio of C1- and C4-oxidized products released by the two LPMOs exhibiting mixed C1/C4-oxidation, *Ta*AA9A (without CBM) and *Tr*AA9A (with CBM). Both LPMOs released predominantly C4-oxidized products, the C4-oxidized fraction of the total solubilized oxidized products being 74–90 % for *Ta*AA9A and 72–94 % for *Tr*AA9A and, when averaged across the three substrate types (Fig. 7A). The ratio of C1- and C4-oxidized products varied slightly with cellulose type. For *Ta*AA9A, the C1:C4 ratio was 11:89 for Cel I, 22:78 for PASC, and 17:83 for Cel II

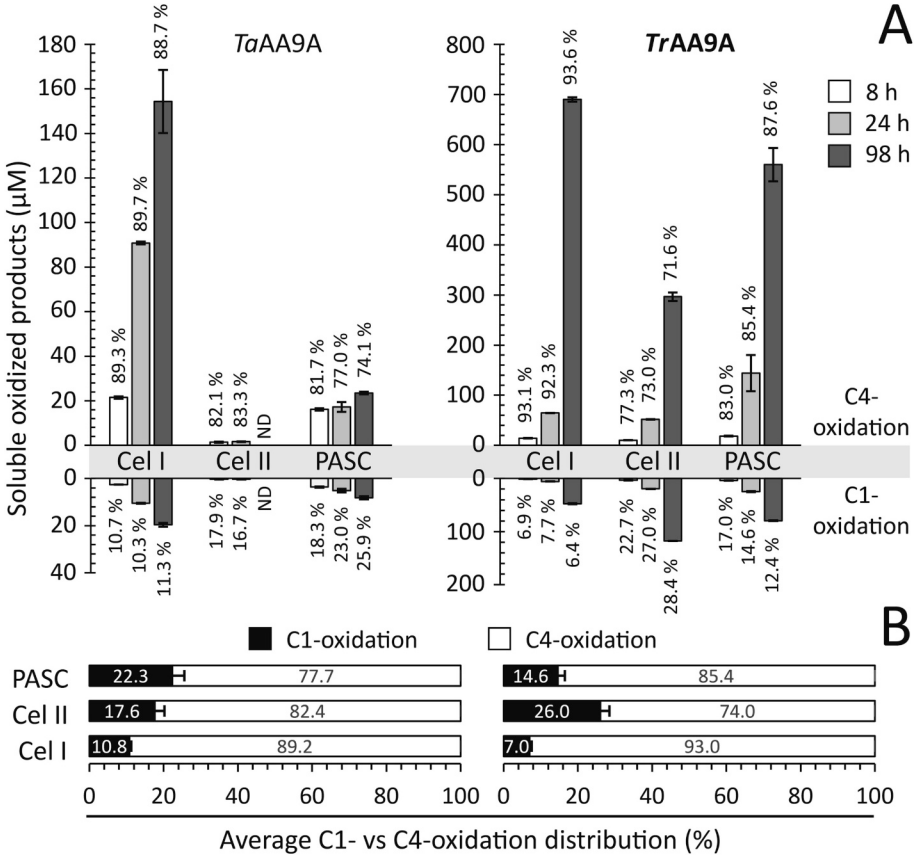

Fig. 7. Substrate-dependent variation in the ratio of soluble C1- and C4-oxidized products. (A) The figure shows the fractions of soluble C1-oxidized (downwards) and C4-oxidized (upwards) products generated by the two C1/C4-oxidizing LPMOs, *Ta*AA9A (without CBM) or *Tr*AA9A (with CBM1), in reactions with Cel I, Cel II, or amorphous cellulose (PASC) after 8 h (white bars), 24 h (light grey bars), and 98 h (dark grey bars). Error bars represent standard deviations derived from two independent reactions. (B) The ratio of C1-oxidized (black) and C4-oxidized (white) products in the supernatant after taking the average of the three time points. Error bars represent standard deviations derived from four (*Ta*AA9A on Cel II) or six independent reactions. ND, not determined.

when taking the average for the samples taken at different time points (Fig. 7B). In comparison, for *Tr*AA9A the C1:C4 ratios were 7:93, 15:85 and 26:74 for Cel I, PASC, and Cel II, respectively (Fig. 7B).

Some of the data sets showed significant variation in the C1:C4 ratio over time, namely for *Ta*AA9A acting on PASC (single factor ANOVA; $p = 0.01448$) and for *Tr*AA9A acting on Cel II and PASC (single factor ANOVA; $p = 0.01362$ and $p = 0.006527$, respectively). The C1:C4 ratio is likely determined by how exactly the LPMO's active site is oriented relative to the scissile glycosidic bond (Danneels et al., 2019; Forsberg et al., 2018). Since LPMOs interact with a surface rather than with a single polysaccharide chain, it is conceivable that various substrates, with various surfaces (which may change during the reaction) show varying C1/C4 product ratios. Fig. 7 shows that, indeed, substrate-dependent variation occurs, although the effects seem modest. For both LPMOs, and for each of the substrates, C4-oxidation was strongly dominating.

4.5. Cellulosic fiber modification

Using the SEC-MALLS data allowed not only calculation of the number average, M_n, which translates into the changes in DP_n reported in Fig. 4, but also the weight-average, M_w, and the z-average, M_z (Fig. S2). As already alluded to above, the largest reduction of polymer chain length was achieved upon treatment with *Pa*AA9E and the two *Nc*AA9C variants (Fig. S2). Of the three cellulose substrates, almost all LPMOs were most efficient on amorphous cellulose in terms of decreasing the DP_n (Fig. 4). In general, a higher extent of cellulose depolymerization (reflected by the relative decrease in DP_n; Fig. 4) was in good agreement with a higher level of solubilized oxidized oligosaccharides and higher extent of substrate binding (Fig. 3). As for the two cellulose allomorphs, Cel I and Cel II, almost all LPMOs tested were more efficient in reducing chain length of Cel I (Fig. 4) as also shown by the release of soluble products depicted in Fig. 3). This preference for Cel I is not surprising, considering that Cel I is the natural allomorph of cellulose.

A closer look at the relative reduction in the molar mass parameters of cellulose substrates after treatment with C4-oxidizing LPMOs (Fig. 8) reveals that M_w and M_z were reduced to a higher extent in reactions with PASC compared to Cel I and Cel II. Furthermore, despite the similar level of reduction in M_n for all three substrates, M_z remained essentially unchanged for Cel II as opposed to Cel I and amorphous cellulose, showing that degradation of Cel II, a non-natural form of cellulose, differs from the degradation of Cel I and PASC.

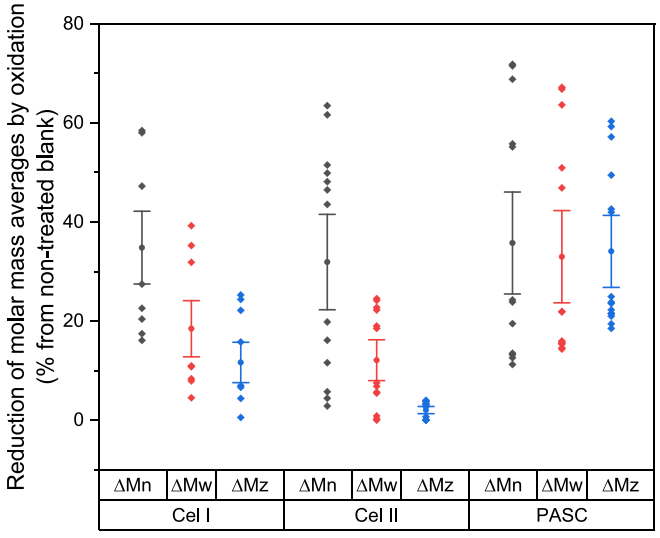

Fig. 8. Reduction of molar mass averages of three cellulose types after treatment with C4-oxidizing LPMOs. Each diamond represents a separate reaction, incubated for 8, 24, or 98 h with a C4-oxidizing LPMO (*un*AA9–1, *Ls*AA9A, *Nc*AA9C, and *Nc*AA9C-N). The bullet with error bar indicates the average value and the 95 % confidence interval thereof, respectively. Underlying data are shown in Fig. S2.

Interestingly, the CBM-free *Nc*AA9C-N variant reduced the molar mass parameters (i.e., M_n, M_w, and M_z) of all three cellulose types to a higher extent than the naturally CBM-containing variant in the early phase of the reaction (after 8 and 24 h, i.e., before enzyme inactivation; Fig. S2). At the same time, *Nc*AA9C-N released less oxidized oligosaccharides, suggesting a difference in the pattern of oxidation between LPMO variants with and without CBM (Figs. 3 & 4). Higher amounts of solubilized oligosaccharides together with a low reduction of molar mass parameters likely relate to the fact that a CBM-containing LPMO catalyzes more localized cleavages (close to the CBM-binding point, which would lead to a bigger chance of the same cellulose chain being cleaved twice, which is a prerequisite for soluble products to emerge (Courtade et al., 2018)).

5. Discussion

Cellulose occurs in various forms and, while LPMOs have been tested primarily with amorphous substrates, a growing number of studies address the application of LPMOs in cellulose fiber engineering (Karnaouri et al., 2022). These studies have focused on Cel I-type fibers, including bleached and unbleached softwood kraft pulp, delignified softwood fibers, and kraft fibers from a variety of plant species, but also grass-type biomass and model celluloses such as Avicel and cotton linters (Koskela et al., 2019; Marjamaa et al., 2022; Moreau et al., 2019; Villares et al., 2017). LPMO treatment has been shown to facilitate mechanical delamination of cellulose fibers (Marjamaa et al., 2023; Villares et al., 2017), degrade surface structures that restrict swelling (Marjamaa et al., 2022), improve production yield of cellulose nanocrystals (CNC) and cellulose nanofibrils (CNF) (Moreau et al., 2019), and change properties of CNC, including water vapor transmission (Marjamaa et al., 2023), mechanical properties (Koskela et al., 2019), and self-organizing properties (Koskela, Wang, Fowler, Tan, & Zhou, 2021). The observed changes in fiber properties after LPMO treatment relate to the introduction of carboxyl groups by C1-type oxidation or carbonyl groups by C4-type oxidation, with both modifications disrupting the crystalline structure of cellulose elementary fibrils (Vermaas, Crowley, Beckham, & Payne, 2015; Villares et al., 2017). In addition, C1-oxidation increases surface charge and, consequently, colloidal stability (Hu, Tian, Renneckar, & Saddler, 2018).

The ability to directly assess and quantify LPMO action on cellulose fibers, i.e., the formation of terminal 1-carboxyl and 4-carbonyl groups, is essential for understanding and controlling fiber oxidation using LPMOs. Methods for quantification of the carboxyl and aldehyde contents of fibers are well established for pulp analysis. As an example, conductometric titration of the carboxyl groups (Hu et al., 2018) and oxidation of the reducing end aldehyde groups with 2,3,5-triphenyl-2H-tetrazolium chloride (TTC) (Ceccherini et al., 2021) have been adapted and applied for assessing LPMO treatment of fibers. Furthermore, selective fluorescence labeling methods have been developed for quantification of 1-carboxyl (Budischowsky et al., 2022; Vuong, Liu, Sandgren, & Master, 2017) and reducing-end aldehyde (Röhrling et al., 2002; Velleste, Teugjas, & Väljamäe, 2010) groups in the fiber fraction. Analysis of 4-carbonyl groups has been lagging as 4-carbonyl oxidation at the nonreducing end of cellulose chains is uncommon in pulps. In this work, we applied the recently developed, first-of-a-kind method that measures C4 oxidation by LPMOs directly and in parallel with cellulose molecular mass, based on size-exclusion chromatography of the dissolved fibers after fluorescence labeling of 4-carbonyl groups generated by the action of C4-oxidizing LPMOs (Sulaeva et al., 2023). As the derivatization method is valid for all cellulose types, we were able to evaluate the impact of a selection of C4-oxidizing LPMOs on Cel I, Cel II, and amorphous cellulose.

The large sequence diversity among fungal AA9-type LPMOs (Lenfant et al., 2017; Várnai et al., 2021) and their general abundance suggest that there may be considerable functional variation among these enzymes, even among enzymes known as "cellulose-active". Such variation may eventually allow assembly of a toolbox with multiple LPMOs for fine-tuned cellulose fiber engineering. Combining fiber analysis with quantification of soluble oxidized products indeed revealed large functional variation between the LPMOs studied here, including the ratio of soluble and insoluble oxidized products, the ability to bind to and act on different cellulose types, and operational stability of the enzyme. Next to showing remarkable functional variation, the present data strengthen the ideas that the ratio of soluble and insoluble products, and thus the nature of fiber modification, depends on the presence of a CBM (this study; (Courtade et al., 2018)) and the reaction conditions, including substrate loading (this study; (Courtade et al., 2018)), enzyme dose (Vuong et al., 2017), and reaction time (this study). While the extent of fiber oxidation was LPMO-dependent and could not be predicted from the amount of soluble oxidized oligosaccharides, accumulation of LPMO-derived soluble oligosaccharides, or the halt thereof, was a good indicator for LPMO activity, or the lack thereof, on the fiber fraction.

The present results confirm for all three studied cellulose types that substrate binding, either by the catalytic domain itself or by an appended CBM, is correlated with catalytic efficiency and is essential for retaining LPMO activity in turnover conditions. Similar observations have been reported by Koskela et al. (Koskela et al., 2019), who showed that a CBM1-carrying AA9 LPMO (*Nc*LPMO9E) remains active longer than a single-domain AA9 LPMO (*Nc*LPMO9F) when oxidizing delignified softwood spruce fibers. Interestingly, we observed variation in the extent of substrate binding between CBM1-carrying LPMOs, which may be tied to sequence variations and/or post-translational modifications of the CBM1 domain. For example, CBM1-containing *un*AA9–1 bound to all three cellulose variants to a much lesser extent compared to CBM1-containing of *Nc*AA9C.

The importance of CBMs for binding to Cel I-type or amorphous cellulose and, consequently, for LPMO stability under turnover conditions has previously been demonstrated for *Sc*AA10C from *Streptomyces coelicolor* (Courtade et al., 2018), *Cf*LPMO10 from *Cellulomonas fimi* (Crouch et al., 2016) and *Tb*LPMO10 from *Thermobispora bispora* (Crouch et al., 2016). The latter study points at the possibility that LPMO action may be tuned by CBM engineering or by replacing one CBM type by another. The present data confirm the results of Courtade et al., who have shown that CBM-free LPMOs lead to more random oxidation patterns, which is reflected in lesser production of soluble oxidized products (Courtade et al., 2018). Here, this notion is strengthened by the observed differences in molar mass distribution of fibers treated with *Nc*AA9C variants that were consistent with more localized action of the CBM-containing LPMO and more dispersed oxidation in the absence of a CBM, for all three cellulose types.

Regarding the potential of LPMOs in fiber engineering, co-quantification of the oxidized products in the fiber fraction and the reaction supernatant clearly indicates the formation of a limited number of oxidized sites in the fibers, and that this number varies among LPMOs and fiber types. Whether fiber oxidation can be achieved beyond this limit, e.g. by combining multiple LPMOs in one reaction, remains to be elucidated. As for Cel II, which is found in regenerated cellulose, only the two *Nc*AA9C variants, *Tr*AA9A, *Pa*AA9E, and *Ls*AA9A were able to bind to, oxidize, and depolymerize this substrate substantially. Of these LPMOs, the two *Nc*AA9C variants and *Ls*AA9A have been shown to act on soluble substrates including cello-oligosaccharides (Isaksen et al., 2014), indicating that the ability to act on single, short cellulose chains may be beneficial for engineering Cel II-type fibers.

The combined analytics of our study highlight differences among LPMOs in terms of the distribution of oxidized groups on the fiber surface and fiber oxidation potential, paving the way for further development of LPMO-based cellulose fiber engineering. Importantly, the current data were obtained using high enzyme dosages and long reaction times, with considerable enzyme inactivation in some cases. Cost-reducing optimization of the LPMO reactions is likely needed to achieve economically sustainable processes. Moreover, the complex relation between substrate binding, co-substrate generation, and stability of LPMOs have implications for the industrial application of LPMOs (Eijsink et al., 2019; Müller, Chylenski, Bissaro, Eijsink, & Horn, 2018). Thus, next to being able to optimally modify cellulose, the suitability of LPMOs to act under process conditions with industrially acceptable efficiency needs attention.

6. Concluding remarks

Fiber modification and pretreatment of cellulosic substrates for the production of cellulose-based materials, such as CNC and CNF, with the use of LPMOs is a rapidly growing field, as LPMO treatment offers an environmentally friendly solution compared to conventional chemical methods. The present study highlights the high variation in the potential of LPMOs for engineering various types of cellulose fibers and reveals some of the underlying features determining LPMO efficacy, including substrate morphology and crystallinity as well as enzyme modularity. Fiber yield loss (indicated by the solubilization of oxidized cello-oligosaccharides), the degree of cellulose fiber depolymerization, and the amount of oxidized sites remaining on the fiber appear to be LPMO specific and are affected by the presence of CBMs. In agreement with previous studies (Courtade et al., 2018; Koskela et al., 2019), our data indicate that single-domain LPMOs, or the single-domain variant of CBM-containing LPMOs, oxidize fibers to a higher extent than CBM-containing LPMOs and release less soluble products, thus retaining a higher pulp yield after LPMO treatment. In conclusion, our study shows great functional variation among cellulose-active LPMOs that may be biologically relevant since such variation may be needed to attack complex natural cellulose-containing materials, with varying topological requirements of the microfibril surfaces. This variation shows that the impact of LPMO treatment in the production of cellulose-based materials will be strongly LPMO-dependent. Harnessing this functional variation and our increased understanding thereof will help maximizing the already demonstrated positive impact of LPMO treatments in cellulose fiber processing.

CRediT authorship contribution statement

Fredrik G. Støpamo: Writing – review & editing, Writing – original draft, Visualization, Investigation, Formal analysis, Conceptualization. **Irina Sulaeva:** Writing – review & editing, Writing – original draft, Visualization, Supervision, Investigation, Formal analysis. **David Budischowsky:** Writing – review & editing, Investigation, Formal analysis. **Jenni Rahikainen:** Writing – review & editing, Visualization, Investigation, Formal analysis. **Kaisa Marjamaa:** Writing – review & editing, Writing – original draft, Supervision, Project administration, Funding acquisition, Conceptualization. **Antje Potthast:** Writing – review & editing, Supervision, Project administration, Funding acquisition, Conceptualization. **Kristiina Kruus:** Writing – review & editing, Funding acquisition, Conceptualization. **Vincent G.H. Eijsink:** Writing – review & editing, Writing – original draft, Supervision, Project administration, Funding acquisition, Conceptualization. **Anikó Várnai:** Writing – review & editing, Writing – original draft, Supervision, Project administration, Funding acquisition, Conceptualization.

Declaration of competing interest

The authors declare that they have no known competing financial interests or personal relationships that could have appeared to influence the work reported in this paper.

Data availability

Data will be made available on request.

Acknowledgements

This work was supported by the European Union's Horizon 2020 research and innovation programme under the umbrella of ERA-NET Cofund Action ForestValue [FunEnzFibres, grant agreement no. 773324] through funding from the Research Council of Norway [grant agreement no. 297907], the Academy of Finland [grant agreement no. 326359], and the Austrian Federal Ministry of Agriculture, Forestry, Environment and Water Management (BMLFUW) [grant agreement no. 101379]. The work was co-funded by the NorBioLab infrastructure grant [grant agreement no. 270038] from the Research Council of Norway. Anikó Várnai also acknowledges the Novo Nordisk Foundation for an Emerging Investigator Grant [grant no. NNF-0061165]. VTT thanks Tiina Pöhler for advice regarding to the BET surface area analysis and Riitta Alander, Mari Leino and Mirja Muhola for technical assistance and expresses gratitude to support by the FinnCERES Materials Bioeconomy Ecosystem. We thank Kasper Bay Tingsted and Pedro Emanuel Garcia Loureiro from Novozymes for providing enzymes.

Appendix A. Supplementary data

Supplementary data to this article can be found online at https://doi.org/10.1016/j.carbpol.2024.121816.

References

Beeson, W. T., Phillips, C. M., Cate, J. H., & Marletta, M. A. (2012). Oxidative cleavage of cellulose by fungal copper-dependent polysaccharide monooxygenases. *Journal of the American Chemical Society, 134*(2), 890–892.

Bissaro, B., Røhr, Å. K., Müller, G., Chylenski, P., Skaugen, M., Forsberg, Z., & Eijsink, V. G. H. (2017). Oxidative cleavage of polysaccharides by monocopper enzymes depends on H_2O_2. *Nature Chemical Biology, 13*, 1123–1128.

Borisova, A. S., Isaksen, T., Dimarogona, M., Kognole, A. A., Mathiesen, G., Várnai, A., & Eijsink, V. G. H. (2015). Structural and functional characterization of a lytic polysaccharide monooxygenase with broad substrate specificity. *The Journal of Biological Chemistry, 290*(38), 22955–22969.

Budischowsky, D., Sulaeva, I., Hettegger, H., Ludwig, R., Rosenau, T., & Potthast, A. (2022). Fluorescence labeling of C1-oxidized cellulose. Part 1: Method development. *Carbohydrate Polymers, 295*, Article 119860.

Carpita, N. C., & McCann, M. C. (2020). Redesigning plant cell walls for the biomass-based bioeconomy. *The Journal of Biological Chemistry, 295*(44), 15144–15157.

Ceccherini, S., Rahikainen, J., Marjamaa, K., Sawada, D., Grönqvist, S., & Maloney, T. (2021). Activation of softwood Kraft pulp at high solids content by endoglucanase and lytic polysaccharide monooxygenase. *Industrial Crops and Products, 166*, Article 113463.

Chalak, A., Villares, A., Moreau, C., Haon, M., Grisel, S., d'Orlando, A., & Berrin, J. G. (2019). Influence of the carbohydrate-binding module on the activity of a fungal AA9 lytic polysaccharide monooxygenase on cellulosic substrates. *Biotechnology for Biofuels, 12*, 206.

Courtade, G., Forsberg, Z., Heggset, E. B., Eijsink, V. G. H., & Aachmann, F. L. (2018). The carbohydrate-binding module and linker of a modular lytic polysaccharide monooxygenase promote localized cellulose oxidation. *The Journal of Biological Chemistry, 293*(34), 13006–13015.

Crouch, L. I., Labourel, A., Walton, P. H., Davies, G. J., & Gilbert, H. J. (2016). The contribution of non-catalytic carbohydrate binding modules to the activity of lytic polysaccharide monooxygenases. *The Journal of Biological Chemistry, 291*(14), 7439–7449.

Danneels, B., Tanghe, M., & Desmet, T. (2019). Structural features on the substrate-binding surface of fungal lytic polysaccharide monooxygenases determine their oxidative regioselectivity. *Biotechnology Journal, 14*(3), Article e1800211.

Drula, E., Garron, M.-L., Dogan, S., Lombard, V., Henrissat, B., & Terrapon, N. (2022). The carbohydrate-active enzyme database: Functions and literature. *Nucleic Acids Research, 50*(D1), D571–D577.

Eijsink, V. G. H., Petrović, D., Forsberg, Z., Mekasha, S., Røhr, Å. K., Várnai, A., & Vaaje-Kolstad, G. (2019). On the functional characterization of lytic polysaccharide monooxygenases (LPMOs). *Biotechnology for Biofuels, 12*(1), 58.

Forsberg, Z., Bissaro, B., Gullesen, J., Dalhus, B., Vaaje-Kolstad, G., & Eijsink, V. G. H. (2018). Structural determinants of bacterial lytic polysaccharide monooxygenase functionality. *The Journal of Biological Chemistry, 293*(4), 1397–1412.

Forsberg, Z., Rohr, A. K., Mekasha, S., Andersson, K. K., Eijsink, V. G., Vaaje-Kolstad, G., & Sorlie, M. (2014). Comparative study of two chitin-active and two cellulose-active AA10-type lytic polysaccharide monooxygenases. *Biochemistry, 53*(10), 1647–1656.

Gupta, G. K., & Shukla, P. (2020). Lignocellulosic biomass for the synthesis of nanocellulose and its eco-friendly advanced applications. *Frontiers. Chemistry, 8*.

Henriksson, M., & Berglund, L. A. (2007). Structure and properties of cellulose nanocomposite films containing melamine formaldehyde. *Journal of Applied Polymer Science, 106*(4), 2817–2824.

Hu, J., Tian, D., Renneckar, S., & Saddler, J. N. (2018). Enzyme mediated nanofibrillation of cellulose by the synergistic actions of an endoglucanase, lytic polysaccharide monooxygenase (LPMO) and xylanase. *Scientific Reports, 8*(1), 3195.

Isaksen, T., Westereng, B., Aachmann, F. L., Agger, J. W., Kracher, D., Kittl, R., & Horn, S. J. (2014). A C4-oxidizing lytic polysaccharide monooxygenase cleaving both cellulose and cello-oligosaccharides. *The Journal of Biological Chemistry, 289*(5), 2632–2642.

Jusner, P., Bacher, M., Simon, J., Bausch, F., Khaliliyan, H., Schiehser, S., & Rosenau, T. (2022). Analyzing the effects of thermal stress on insulator papers by solid-state 13C NMR spectroscopy. *Cellulose, 29*(2), 1081–1095.

Karnaouri, A., Chorozian, K., Zouraris, D., Karantonis, A., Topakas, E., Rova, U., & Christakopoulos, P. (2022). Lytic polysaccharide monooxygenases as powerful tools in enzymatically assisted preparation of nano-scaled cellulose from lignocellulose: A review. *Bioresource Technology, 345*, Article 126491.

Ketola, A., Hjelt, T., Lappalainen, T., Pajari, H., Tammelin, T., Salminen, K., Lee, K.-Y., Rojas, O.J., & Ketoja, J.A. (2022). The relation between bubble-fibre interaction and material properties in foam forming. In Coffin, D.W. & Batchelor, W.J. (Eds.), Advances in pulp and paper research, Cambridge 2022: Transactions of the 17th fundamental research symposium (pp. 65-84). Oxfordshire; The Pulp and Paper Fundamental Research Society.

Kittl, R., Kracher, D., Burgstaller, D., Haltrich, D., & Ludwig, R. (2012). Production of four *Neurospora crassa* lytic polysaccharide monooxygenases in *Pichia pastoris* monitored by a fluorimetric assay. *Biotechnology for Biofuels, 5*(1), 79.

Kont, R., Pihlajaniemi, V., Borisova, A. S., Aro, N., Marjamaa, K., Loogen, J., & Väljamäe, P. (2019). The liquid fraction from hydrothermal pretreatment of wheat straw provides lytic polysaccharide monooxygenases with both electrons and H_2O_2 co-substrate. *Biotechnology for Biofuels, 12*, 235.

Koskela, S., Wang, S., Fowler, P. M. P., Tan, F., & Zhou, Q. (2021). Structure and self-assembly of lytic polysaccharide monooxygenase-oxidized cellulose nanocrystals. *ACS Sustainable Chemistry & Engineering, 9*(34), 11331–11341.

Koskela, S., Wang, S., Xu, D., Yang, X., Li, K., Berglund, L. A., & Zhou, Q. (2019). Lytic polysaccharide monooxygenase (LPMO) mediated production of ultra-fine cellulose nanofibres from delignified softwood fibres. *Green Chemistry, 21*(21), 5924–5933.

Lansing, W. D., & Kraemer, E. O. (1935). Molecular weight analysis of mixtures by sedimentation equilibrium in the Svedberg ultracentrifuge. *Journal of the American Chemical Society, 57*(7), 1369–1377.

Lenfant, N., Hainaut, M., Terrapon, N., Drula, E., Lombard, V., & Henrissat, B. (2017). A bioinformatics analysis of 3400 lytic polysaccharide oxidases from family AA9. *Carbohydrate Research, 448*, 166–174.

Li, J., Solhi, L., Goddard-Borger, E. D., Mathieu, Y., Wakarchuk, W. W., Withers, S. G., & Brumer, H. (2021). Four cellulose-active lytic polysaccharide monooxygenases from *Cellulomonas* species. *Biotechnology for Biofuels, 14*(1), 29.

Ling, Z., Wang, T., Makarem, M., Santiago Cintrón, M., Cheng, H. N., Kang, X., & French, A. D. (2019). Effects of ball milling on the structure of cotton cellulose. *Cellulose, 26*(1), 305–328.

Liu, Y., Shi, L., Cheng, D., & He, Z. (2016). Dissolving pulp market and technologies: Chinese prospective – A mini-review. *BioResources, 11*(3), 7902–7916.

Loose, J. S. M., Forsberg, Z., Fraaije, M. W., Eijsink, V. G. H., & Vaaje-Kolstad, G. (2014). A rapid quantitative activity assay shows that the *Vibrio cholerae* colonization factor GbpA is an active lytic polysaccharide monooxygenase. *FEBS Letters, 588*, 3435–3440.

Loureiro, P. E. G., Cadete, S. M. S., Tokin, R., Evtuguin, D. V., Lund, H., & Johansen, K. S. (2021). Enzymatic fibre modification during production of dissolving wood pulp for regenerated cellulosic materials. *Frontiers. Plant Science, 12*.

Marjamaa, K., & Kruus, K. (2018). Enzyme biotechnology in degradation and modification of plant cell wall polymers. *Physiologia Plantarum, 164*(1), 106–118.

Marjamaa, K., Lahtinen, P., Arola, S., Maiorova, N., Nygren, H., Aro, N., & Koivula, A. (2023). Oxidative treatment and nanofibrillation softwood Kraft fibres with lytic polysaccharide monooxygenases from *Trichoderma reesei* and *Podospora anserina*. *Industrial Crops and Products, 193*, Article 116243.

Marjamaa, K., Rahikainen, J., Karjalainen, M., Maiorova, N., Holopainen-Mantila, U., Molinier, M., & Kruus, K. (2022). Oxidative modification of cellulosic fibres by lytic polysaccharide monooxygenase AA9A from *Trichoderma reesei*. *Cellulose, 29*(11), 6021–6038.

Moilanen, U., Kellock, M., Várnai, A., Andberg, M., & Viikari, L. (2014). Mechanisms of laccase-mediator treatments improving the enzymatic hydrolysis of pre-treated spruce. *Biotechnology for Biofuels, 7*(1), 177.

Moreau, C., Tapin-Lingua, S., Grisel, S., Gimbert, I., Le Gall, S., Meyer, V., & Villares, A. (2019). Lytic polysaccharide monooxygenases (LPMOs) facilitate cellulose nanofibrils production. *Biotechnology for Biofuels, 12*, 156.

Müller, G., Chylenski, P., Bissaro, B., Eijsink, V. G. H., & Horn, S. J. (2018). The impact of hydrogen peroxide supply on LPMO activity and overall saccharification efficiency of a commercial cellulase cocktail. *Biotechnology for Biofuels, 11*, 209.

Müller, G., Várnai, A., Johansen, K. S., Eijsink, V. G. H., & Horn, S. J. (2015). Harnessing the potential of LPMO-containing cellulase cocktails poses new demands on processing conditions. *Biotechnology for Biofuels, 8*, 187.

Østby, H., Christensen, I. A., Hennum, K., Várnai, A., Buchinger, E., Grandal, S., & Eijsink, V. G. H. (2023). Functional characterization of a lytic polysaccharide monooxygenase from *Schizophyllum commune* that degrades non-crystalline substrates. *Scientific Reports, 13*, 17373.

Phillips, C. M., Beeson, W. T., Cate, J. H., & Marletta, M. A. (2011). Cellobiose dehydrogenase and a copper-dependent polysaccharide monooxygenase potentiate cellulose degradation by *Neurospora crassa*. *ACS Chemical Biology, 6*(12), 1399–1406.

Quinlan, R. J., Sweeney, M. D., Lo Leggio, L., Otten, H., Poulsen, J. C., Johansen, K. S., & Walton, P. H. (2011). Insights into the oxidative degradation of cellulose by a copper metalloenzyme that exploits biomass components. *Proceedings of the National Academy of Sciences of the United States of America, 108*(37), 15079–15084.

Rahikainen, J., Ceccherini, S., Molinier, M., Holopainen-Mantila, U., Reza, M., Väisänen, S., & Grönqvist, S. (2019). Effect of cellulase family and structure on modification of wood fibres at high consistency. *Cellulose, 26*(8), 5085–5103.

Revol, J. F., Dietrich, A., & Goring, D. A. I. (1987). Effect of mercerization on the crystallite size and crystallinity index in cellulose from different sources. *Canadian Journal of Chemistry, 65*(8), 1724–1725.

Röder, T., Moosbauer, J., Fasching, M., Bohn, A., Fink, H.-P., Baldinger, T., & Sixta, H. (2006). Crystallinity determination of native cellulose - comparison of analytical methods. *Lenzinger Berichte, 86*, 132–136.

Röhrling, J., Potthast, A., Rosenau, T., Lange, T., Ebner, G., Sixta, H., & Kosma, P. (2002). A novel method for the determination of carbonyl groups in cellulosics by fluorescence labeling. 1. Method development. *Biomacromolecules, 3*(5), 959–968.

Sheldon, R. A. (2016). Green chemistry, catalysis and valorization of waste biomass. *Journal of Molecular Catalysis A: Chemical, 422*, 3–12.

Simmons, T. J., Frandsen, K. E. H., Ciano, L., Tryfona, T., Lenfant, N., Poulsen, J. C., & Dupree, P. (2017). Structural and electronic determinants of lytic polysaccharide monooxygenase reactivity on polysaccharide substrates. *Nature Communications, 8*(1), 1064.

Solhi, L., Li, J., Li, J., Heyns, N. M. I., & Brumer, H. (2022). Oxidative enzyme activation of cellulose substrates for surface modification. *Green Chemistry, 24*(10), 4026–4040.

Ståhlberg, J., Divne, C., Koivula, A., Piens, K., Claeyssens, M., Teeri, T. T., & Jones, T. A. (1996). Activity studies and crystal structures of catalytically deficient mutants of cellobiohydrolase I from *Trichoderma reesei*. *Journal of Molecular Biology, 264*(2), 337–349.

Sulaeva, I., Budischowsky, D., Rahikainen, J., Marjamaa, K., Støpamo, F. G., Khaliliyan, H., & Potthast, A. (2023). A novel approach to analyze the impact of lytic polysaccharide monooxygenases (LPMOs) on cellulosic fibres. *Carbohydrate Polymers, 328*, Article 121696.

Sun, P., Valenzuela, S. V., Chunkrua, P., Javier Pastor, F. I., Laurent, C. V. F. P., Ludwig, R., & Kabel, M. A. (2021). Oxidized product profiles of AA9 lytic polysaccharide monooxygenases depend on the type of cellulose. *ACS Sustainable Chemistry & Engineering, 9*(42), 14124–14133.

Swerin, A., Odberg, L., & Lindström, T. (1990). Deswelling of hardwood kraft pulp fibers by cationic polymers. *The effect on wet pressing and sheet properties, 5*(4), 188–196.

Tuveng, T. R., Jensen, M. S., Fredriksen, L., Vaaje-Kolstad, G., Eijsink, V. G. H., & Forsberg, Z. (2020). A thermostable bacterial lytic polysaccharide monooxygenase with high operational stability in a wide temperature range. *Biotechnology for Biofuels, 13*(1), 194.

Vaaje-Kolstad, G., Westereng, B., Horn, S. J., Liu, Z., Zhai, H., Sørlie, M., & Eijsink, V. G. H. (2010). An oxidative enzyme boosting the enzymatic conversion of recalcitrant polysaccharides. *Science, 330*(6001), 219–222.

Várnai, A., Hegnar, O. A., Horn, S. J., Eijsink, V. G. H., & Berrin, J.-G. (2021). Fungal lytic polysaccharide monooxygenases (LPMOs): Biological importance and applications. In O. Zaragoza (Ed.), *Encyclopedia of mycology* (pp. 281–294). Oxford: Elsevier.

Velleste, R., Teugjas, H., & Väljamäe, P. (2010). Reducing end-specific fluorescence labeled celluloses for cellulase mode of action. *Cellulose, 17*(1), 125–138.

Vermaas, J. V., Crowley, M. F., Beckham, G. T., & Payne, C. M. (2015). Effects of lytic polysaccharide monooxygenase oxidation on cellulose structure and binding of oxidized cellulose oligomers to cellulases. *The Journal of Physical Chemistry. B, 119*(20), 6129–6143.

Villares, A., Moreau, C., Bennati-Granier, C., Garajova, S., Foucat, L., Falourd, X., & Cathala, B. (2017). Lytic polysaccharide monooxygenases disrupt the cellulose fibers structure. *Scientific Reports, 7*, 40262.

Vuong, T. V., Liu, B., Sandgren, M., & Master, E. R. (2017). Microplate-based detection of lytic polysaccharide monooxygenase activity by fluorescence-labeling of insoluble oxidized products. *Biomacromolecules, 18*(2), 610–616.

Wingren, A., Galbe, M., & Zacchi, G. (2003). Techno-economic evaluation of producing ethanol from softwood: Comparison of SSF and SHF and identification of bottlenecks. *Biotechnology Progress, 19*(4), 1109–1117.

Wood, T. M. (1988). Preparation of crystalline, amorphous, and dyed cellulase substrates. In *Methods in enzymology* (pp. 19–25). Academic Press.

Yan, L., Kasal, B., & Huang, L. (2016). A review of recent research on the use of cellulosic fibres, their fibre fabric reinforced cementitious, geo-polymer and polymer composites in civil engineering. *Composites Part B: Engineering, 92*, 94–132.

Zámocký, M., Schumann, C., Sygmund, C., O'Callaghan, J., Dobson, A. D., Ludwig, R., & Peterbauer, C. K. (2008). Cloning, sequence analysis and heterologous expression in *Pichia pastoris* of a gene encoding a thermostable cellobiose dehydrogenase from *Myriococcum thermophilum*. *Protein Expression and Purification, 59*(2), 258–265.

Zhang, Y. H. P., Cui, J., Lynd, L. R., & Kuang, L. R. (2006). A transition from cellulose swelling to cellulose dissolution by *o*-phosphoric acid: Evidence from enzymatic hydrolysis and supramolecular structure. *Biomacromolecules, 7*(2), 644–648.

Zimm, B. H. (1948). Apparatus and methods for measurement and interpretation of the angular variation of light scattering; preliminary results on polystyrene solutions. *The Journal of Chemical Physics, 16*(12), 1099–1116.